

Effect of Blade Shape on Aerodynamic and Aeroacoustic characteristics of Vertical Axis Wind Turbines using mid-fidelity and high-fidelity methods

TA Tarun Ramprakash *

Indian Institute of Technology BHU, Varanasi, 221005, India

Shubham Shubham^{† ‡}

Nottingham Trent University, Nottingham, NG1 4FQ, United Kingdom

Cranfield University, Bedford, MK43 0AL, United Kingdom

Anton Ianakiev[§]

Nottingham Trent University, Nottingham, NG1 4FQ, United Kingdom

This research paper investigates the effect of different blade shapes on the aerodynamic and aeroacoustic characteristics of Darrieus Vertical Axis Wind Turbines (VAWTs). Three different VAWT blade shapes are investigated: Straight, Troposkein, and Helical, considering a chord-based Reynolds number of $1.73e+5$ and at a constant tip speed ratio for all. The mid-fidelity Lifting Line Free Vortex Wake (LLFVW) method and the high-fidelity Lattice Boltzmann/Very Large Eddy Simulation (LB-VLES) method are employed. Power performance analysis reveals that the straight-bladed VAWT generates the highest power output (about 11% higher), followed by the helical and troposkein blade configurations. The helical-bladed rotor exhibits smoother thrust and torque distribution over a wider azimuthal angle range, as predicted by both methods. While both methods capture the same trends in thrust and torque values, the mid-fidelity LLFVW method predicts $\sim 22\%$ higher C_T and C_Q values and lower near-wake streamwise velocities as compared to the high-fidelity LBM. The LLFVW is unable to accurately capture the inherent 3D vortices in the VAWT flow-field and the effect of blade-vortex interaction (BVI) on the VAWT force-field, as compared to LBM. In terms of aeroacoustics, the troposkein VAWT produces the highest noise at lower frequencies (20-30 Hz), followed by the straight and helical VAWTs. However, the troposkein and helical VAWTs emit more noise at higher frequencies (500-2000 Hz) than the straight VAWT due to the higher intensity of BVI observed for the former.

I. Nomenclature

c	=	blade chord, m
C_T	=	thrust coefficient
C_{Fz}	=	cross-streamwise force coefficient
C_Q	=	torque coefficient
C_P	=	power coefficient
D	=	VAWT diameter, m
f	=	frequency, Hz
h	=	grid spacing, m
M	=	free-stream Mach number
n	=	rotations per second, 1/s
Q	=	VAWT torque, Nm

*Undergraduate Researcher, tatarun.ramprakash.met20@itbhu.ac.in, AIAA Member 1440185

[†]PhD researcher, Sustainable Energy Systems, Department of Civil Engineering, shubham.shubham@ntu.ac.uk, AIAA member 1345559

[‡]Post-Doctoral Research Fellow, School of Aerospace, Transport and Manufacturing, shubham.shubham@cranfield.ac.uk

[§]Professor, Sustainable Energy Systems, Department of Civil Engineering, anton.ianakiev@ntu.ac.uk

r	=	VAWT radius, m
Re	=	Reynolds number
Re_c	=	chord-based Reynolds number
T	=	VAWT thrust, N
u	=	uncertainty
V_∞	=	freestream velocity, m/s
V_{eff}	=	resultant velocity, m/s
V_{tip}	=	blade tip velocity, m/s
σ	=	VAWT solidity
ω	=	VAWT rotational speed, rad/s
α	=	angle of attack, $^\circ$
λ	=	tip speed ratio
ρ	=	air density, kg/m^3

II. Introduction

The performance of a Vertical Axis Wind Turbine (VAWT), in terms of its aerodynamic and aeroacoustic characteristics, has gained increasing attention in recent times, especially in urban areas. The utilisation of wind energy has garnered increasing attention from both industry and local governments as a viable alternative to conventional, non-renewable electricity generation methods. The focus on sustainability in urban areas has become more significant in recent years, as such areas account for a substantial proportion of a nation's carbon emissions. The United Nations reports that the global urban population is projected to rise by 2.5 billion from 2018 to 2050, which equates to 68% of the world's population residing in urban areas, as opposed to the current 55% [1]. By adopting urban wind turbines as a more sustainable means of energy generation, cities can work towards achieving carbon neutrality. In addition to reducing transmission losses and increasing power generation efficiency [2, 3], localised off-grid systems can raise consumer awareness, thereby enabling them to become energy producers.

Vertical Axis Wind Turbines (VAWTs) are better suited for turbulent and chaotic urban flow conditions compared to Horizontal Axis Wind Turbines (HAWTs) in rural areas. A study conducted by Dabiri [4] has shown that VAWT wind farms in urban areas can generate more power per unit area of the ground than HAWT farms. VAWTs offer advantages like lower cut-in speeds, reduced noise levels, omnidirectionality, and easy maintenance. The most commonly used VAWT design is the Darrieus H-rotor, which consists of vertically rotating straight airfoil-shaped blades. The design of VAWTs significantly influences their aerodynamic and aeroacoustic characteristics, particularly for the Darrieus type. The blade design is a crucial parameter in the design of VAWTs for urban applications [5, 6]. Since Darrieus VAWTs generate torque primarily through the aerodynamic forces on the blades, optimizing the blade shape is a key research objective to maximize energy extraction from the wind. The noise associated with VAWTs is directly related to the aerodynamic forces on the blades, making the choice of blade design critical. Darrieus VAWTs have the potential to increase power generation capacity [7], but addressing wind turbine rotor noise is crucial for the growth of the VAWT market. To overcome certain limitations of VAWTs, such as lower overall efficiency and inability to self-start, the optimal design of the blade shape is of utmost importance.

Sengupta [8] conducted a comprehensive investigation on the influence of blade camber and curvature on the performance of straight-bladed VAWTs. Their study revealed that VAWTs equipped with blades featuring a more rounded profile, characterized by higher curvature on the inner surface and lesser curvature on the outer surface around the aerodynamic moment center, exhibited improved self-starting capability and enhanced power extraction performance. In a separate investigation, Mohamed [9] conducted an extensive numerical study to assess the impact of airfoil shape on the power extraction characteristics of straight-bladed VAWTs. The study examined the power coefficient and efficiency of 20 different symmetric and non-symmetric airfoils. The findings revealed that the straight-bladed VAWT utilizing the S-1046 airfoil design exhibited a substantial improvement of 26.83% in power generation compared to the traditional VAWT employing the conventional NACA airfoil design. In a different approach, Chen et al. [10] developed a unique VAWT design incorporating two sets of blades to enhance both the turbine's starting ability and power coefficient. This design deviation from traditional VAWTs involved the addition of an auxiliary identical straight blade on the radial arm of the turbine. Through a comparative analysis with a conventional wind turbine equipped with a single ring of blades, the torque and power output were evaluated. The results demonstrated that the VAWT with two sets of blades achieved higher static torque, indicating significant improvement in starting ability. However, the power extraction was reduced compared to the VAWT with a single set of blades. These studies provide valuable insights into the influence of blade

characteristics, such as camber, curvature, and airfoil shape, on the performance of VAWTs. Understanding these effects is crucial for optimizing the design and efficiency of VAWTs, ultimately facilitating the adoption of wind energy as a sustainable power generation solution.

Despite the available literature, there is still a lack of comprehensive studies using full 3D high-fidelity numerical simulations on the flow physics of unsteady blade loads and downstream turbulent near-wake of VAWTs, for different blade shapes. Furthermore, the capability of mid-fidelity analytical aerodynamic methods to capture the effects of blade shape on VAWT force and flow field is not well understood. Therefore, this study aims to take the first step towards creating a multi-fidelity simulation framework. This is achieved by conducting high-fidelity 3D aerodynamic simulations using the Lattice Boltzmann Method (LBM) and mid-fidelity simulations using the Lifting Line Free Vortex Wake (LLFVW) method for various blade shapes. Furthermore, in the context of aeroacoustics, there is a research gap in identifying the impact of blade shape on VAWT aeroacoustic performance and noise sources. For this, aeroacoustic post-processing is performed using the Ffowcs Williams and Hawkings (FW-H) methodology to calculate the far-field noise.

The first objective is to compare the results of both methods used and investigate any differences observed. Secondly, the aim is to gain insights into different fluid dynamic interactions which occur due to different blade shapes and their effect on the flow and force field of the VAWT. Finally, the effect of blade shape on VAWT aeroacoustics will also be investigated. High-fidelity simulations enable accurate resolution of flow around VAWT blades and downstream wake to study 3D effects on force and flow field, including non-uniform blade loading and non-uniform wake, dynamic stall, blade-vortex interaction, and wake recovery. On the other hand, the mid-fidelity simulation offers simplified modelling of the flow field using vortex lifting lines and aids in a fundamental understanding of the 3D effects for different blade shapes. A comparative analysis between the two methods can also determine the potential of the mid-fidelity method as a substitute for high-fidelity simulation to save significant time and computational resources. Within the context of this work, three distinct VAWT blade geometries have been examined, specifically the straight, troposkein and helical blade shapes. To have a fair investigation of the different blade shapes, the straight-bladed geometry was adapted from Balduzzi [11] and further blade shapes were modified accordingly for the three configurations, keeping the same swept area.

III. Methodology and Setup

A. Numerical computations

1. Flow solver - QBlade

The lifting line method is used to compute the force and flow field because it was shown to be accurate and efficient for similar low Reynolds number rotor applications [12–14]. The lifting line method belongs to a family of various "vortex methods", the computational cost of which falls somewhere in between low-fidelity momentum methods (BEMT, DMS, etc.) and high-fidelity CFD methods (Navier Stokes, Lattice-Boltzmann). In the present study, the lifting line theory coupled to a free vortex wake model is used to calculate the VAWT three-dimensional (3D) unsteady flow field past the rotor and the interaction between blade and fluid flow [11, 15]. The LLFVW algorithm is based on nonlinear lifting line formulation by Garrel [16] and is mentioned in detail by Balduzzi [11].

The fluid is modelled as incompressible, inviscid and irrotational; the blade is modelled with a single line of vortices which is located on the quarter chord points of the blade. The wake is discretised into vortex line elements (straight or curved) and these elements are shed at the blade trailing edges at every time step. They then undergo free convection past the rotor ("free wake method") in which the position of the wake end nodes is updated based on the local velocity, which is a combination of inflow velocity and induced velocity from all the wake elements in the domain. Nonlinear in the "nonlinear lifting line formulation" means the circulation calculated on the lifting line bound vortices is acquired from the nonlinear airfoil lift and drag data provided as input. Lift and drag forces are then calculated based on the local angle of attack (α).

The vortex elements are desingularised using the van Garrel's cut-off method [17] with the vortex core size, taking into account viscous diffusion via the vortex core size that is modelled through the kinematic viscosity ν , a turbulent vortex viscosity coefficient δ_ν , and a time offset parameter S_c using the below equation:

$$r_c = \left(\frac{5.03\delta_\nu\nu(t + S_c)}{1 + \varepsilon} \right)^{1/2} \quad (1)$$

The effects of unsteady aerodynamics and dynamic stall are introduced via the ATEFlap aerodynamic model [18, 19] that reconstructs lift and drag hysteresis curves from a decomposition of the lift polars. The implemented ATEFlap formulation has been further adapted to work under the complex conditions of VAWT exhibiting large fluctuations in the angle of attack when rotating at low TSR [20]. Wake reduction schemes have been implemented to lower computational requirements [18–21]. In the present study, all results with this method will henceforth be referred to with the 'LLFVW' nomenclature.

2. Flow solver - PowerFLOW

The Lattice Boltzmann Method (LBM) is used to compute the force and flow field because it was shown to be accurate and efficient for similar low Reynolds number rotor applications [12, 13, 22–24]. The commercial software 3DS Simulia PowerFLOW has been already validated for aerodynamic and aeroacoustic studies on rotors in general [25–27]. The software solves the discrete Lattice Boltzmann (LB) equation for a finite number of directions. For a detailed description of the method, the reader can refer to Succi [28] and Shan et al. [29], while to Chen and Doolen [30] for a review. The LB method determines the macroscopic flow variables starting from the mesoscopic kinetic equation, i.e. the LB equation. The discretization used for this particular application consists of 19 discrete velocities in three dimensions (D3Q19), involving a third-order truncation of the Chapman-Enskog expansion [31]. The distribution of particles is solved by means of the LB equation on a Cartesian mesh, known as a lattice. An explicit time integration and a collision model are used. For the collision term, the formulation based on a unique Galilean invariant [32] is used. The equilibrium distribution of Maxwell-Boltzmann is adopted [31].

To take into account the effect of the sub-grid unresolved scales of turbulence, a Very Large Eddy Simulation (VLES) model is implemented. Following Yakhot and Orszag [33], a two-equations $k - \epsilon$ Renormalization Group is used to compute a turbulent relaxation time that is added to the viscous relaxation time. To reduce the computational cost, a pressure-gradient-extended wall-model is used to approximate the no-slip boundary condition on solid walls [34, 35]. The model is based on the extension of the generalised law-of-the-wall model [36] to take into account the effect of pressure gradient. These equations are iteratively solved from the first cell close to the wall in order to specify the boundary conditions of the turbulence model. For this purpose, a slip algorithm [30], obtained as generalization of a bounce-back and specular reflection process, is used.

Far-field noise is computed using the Ffowcs Williams and Hawkings [37] (FW-H) acoustic analogy. In particular, the formulation 1A of Farassat and Succi [38] extended to a convective wave equation is used in this study [39]. The formulation has been implemented in the time domain using a source-time dominant algorithm [40]. Pressure fluctuations are recorded on three permeable surfaces enclosing the wind turbine and its wake. These pressure fluctuations are used as input to the FW-H solver, thereby including all noise sources inside the three surfaces. Pressure fluctuations are also captured on all solid surfaces (blade surfaces), which when input to the FW-H solver will include noise sources only on the solid surfaces.

3. Wind turbine geometry

The present study employs the Darrieus VAWT rotor configurations and examines the flow characteristics associated with three distinct blade shapes: Straight, Troposkein, and Helical. Furthermore, various geometrical parameters are adjusted based on a previous study by Balduzzi et al.(2018) [11] to validate the results of this study. The number of blades is fixed for the three configurations so that the study can be focused only on the effect of blade shape on VAWT performance. In the case of helical VAWT, the helix angle (φ) is taken to be 45 degrees, and both Helical and Troposkein geometry was obtained using the spanwise optimization function in QBlade. Figure 1 illustrates the different VAWT configurations used in this study, while Table 1 presents the geometrical values and operational conditions of all three configurations. To have a fair comparison between the three different VAWT configurations, the rotor solidity and the swept area are fixed for all configurations as 0.25 (in the case of troposkein, this is the solidity at the equator) and $1.54m^2$ respectively. The rotor aspect ratio for all configurations is 1.46. There is no central tower or supporting struts used.

Table 1 VAWT geometry and operational settings

	Blade height (H)	Rotor diameter (D)	Chord length (c)	Freestream velocity (V_∞)	Airfoil
VAWT benchmark [11]	1.5 m	1.03 m	0.086 m	9 m/s	NACA 0021

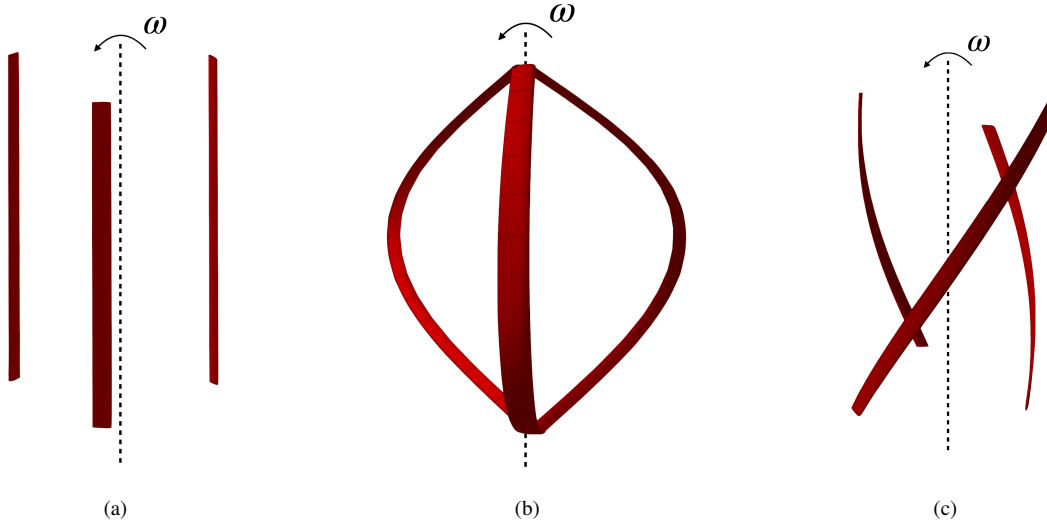


Fig. 1 VAWT Configurations used in this study : (a) Straight (b) Troposkein (c) Helical ($\varphi = 45^\circ$)

The current study employs high-fidelity LBM simulations for all three VAWT configurations. Additionally, each configuration is simulated using the mid-fidelity LLFVW method. Accurate and reliable airfoil data are crucial for obtaining precise results using mid-fidelity aerodynamic methods. To ensure this, a virtual airfoil geometry is derived from the NACA 0021 profile, taking into account the virtual camber effect as described by Rainbird et al. [41]. The transformation of the airfoil is achieved using the conformal transformation technique based on the chord-to-radius ratio, as outlined by Bianchini et al. [42]. Figure 2 (a) illustrates the resulting transformed airfoil. Lift and drag coefficients are obtained for Reynolds numbers ranging from 1×10^5 to 1×10^6 using XFOil [43]. The XFOil calculations employ an $NCrit$ value of nine and forced transition at the leading edge of both the pressure and suction side. The airfoil's static polar data is extrapolated to a 360° range of angle of attack (α) using the Montgomerie method [44] to ensure a smooth extrapolation in the post-stall regime. The same method for 360° polar extrapolation for a VAWT is also used by Balduzzi et al. [11].

4. Numerical setup

For the high-fidelity LBM, a simulation volume is implemented in the form of a cube, with each side measuring $100D$, where D is VAWT diameter. The VAWT geometry is positioned at the centre of the volume. The boundary conditions for the simulation are illustrated in Figure 2 (b). The velocity inlet is specified to have a magnitude of the freestream velocity V_∞ in the direction parallel to the Y-axis. At the pressure outlet, an ambient pressure of 101.325 kPa is imposed. The blade surface is subjected to a no-slip boundary condition.

To generate a volume grid surrounding the solid components within the computational domain, PowerFLOW employs a Cartesian grid approach. This process begins with the minimum hexahedral cell (voxel) size, along with a specified number of variable resolution (VR) levels. The VR levels are organized in a sequence ranging from fine to coarse, with a voxel size ratio of 2 between adjacent VRs, leading to distinct VR regions. The software automatically intersects the Cartesian mesh with the solid components, resulting in a collection of polygons, known as surfels, that accurately represent the body's surface. In order to optimize computational efficiency, the present study adopts 17 VR regions, where higher resolutions are allocated near the blade surface with an offset, while coarser regions are positioned further away from the blade and rotor. This approach enables the allocation of computational resources primarily to areas of interest and where significant flow gradients are expected.

In Figure 2 (b), three red spherical surfaces are depicted, which enclose the flow field of the VAWT rotor. These surfaces serve as FW-H (Ffowcs Williams-Hawkings) permeable boundaries aimed at mitigating hydrodynamic fluctuations within the wake vortices of the VAWT. The averaging of pressure data obtained from all the permeable surfaces contributes to reducing spurious noise sources. The blade surfaces of the VAWT are identified as FW-H solid surfaces. While the utilization of the FW-H permeable formulation is a potential alternative, it has not been employed in this particular study due to the challenges in effectively eliminating spurious noise sources when using only three

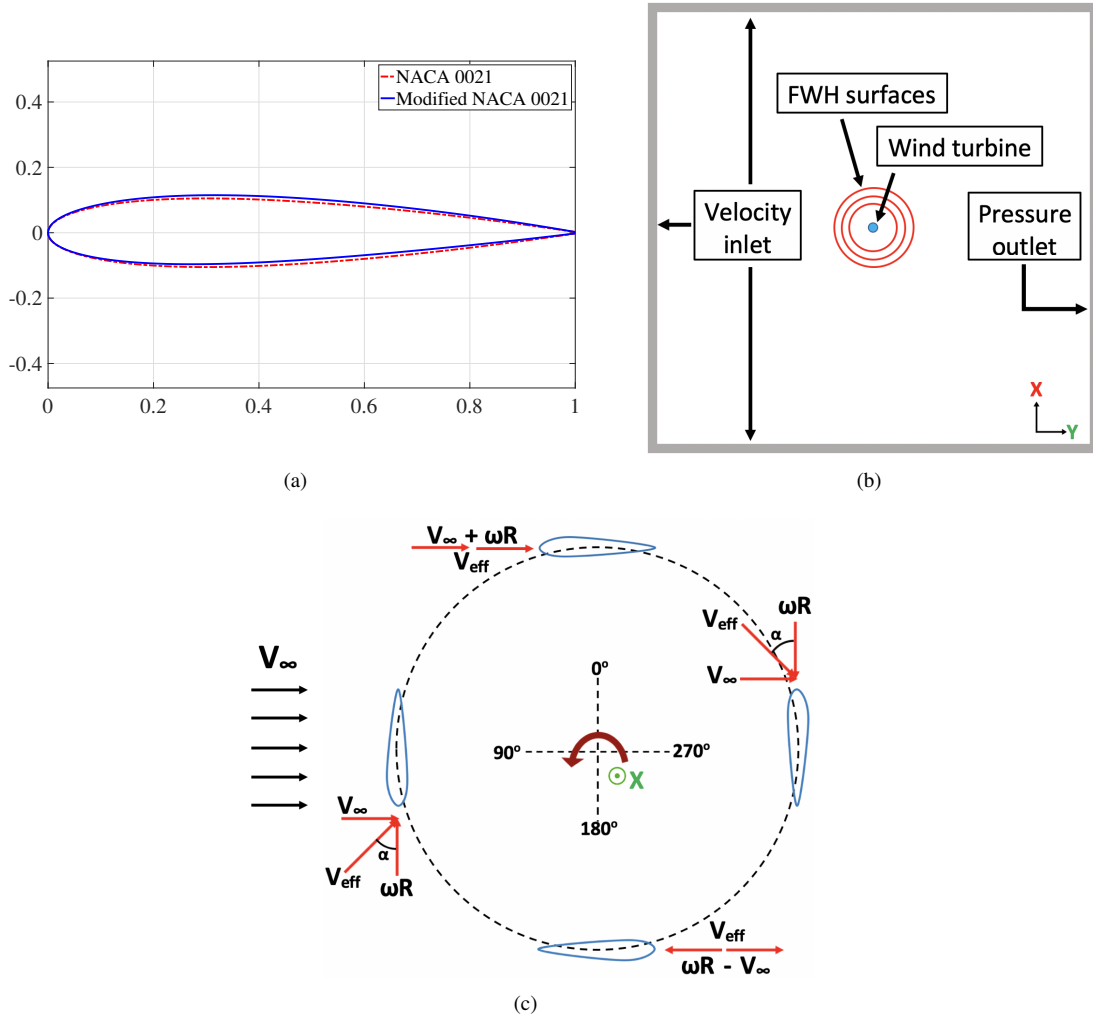


Fig. 2 Computational setup (a) Virtual camber airfoil (Blue) and original airfoil (Red) for mid-fidelity simulation (b) Schematic representation of the simulation domain for High Fidelity LBM (c) Position of Darrieus blades over a single rotation, along with velocity diagram in the blade reference frame (adapted from Shubham et al. [6, 23])

spherical surfaces within the context of a VAWT. In future investigations, a separate examination will be conducted to explore the implementation of the FW-H permeable formulation for VAWT aeroacoustics in a more efficient manner. To ensure accurate capture of acoustic waves, a criterion of a minimum of 15 points per wavelength is adopted, and pressure data is sampled at a rate of 8000 Hz for eight complete rotor rotations. Subsequently, noise spectra are calculated using a Hanning window with a 50% overlap and a frequency resolution (Δf) of 15 Hz.

5. Flow conditions and grid settings

Firstly, for the high-fidelity LBM setup, the VAWT operational setting is presented in Table 2. The tip speed ratio (TSR) is utilized as a metric to characterize the system's operational state. TSR is defined as the ratio of the blade rotational speed (ωR) to the freestream velocity (V_∞), where R denotes the wind turbine radius ω the rotational speed in rad/s. In this study, the freestream velocity is maintained at a constant value of 9 m/s, as per the reference value reported by Balduzzi et al. [11]. The rotational speed (ω) is adjusted to achieve different TSR values, mimicking real-world scenarios where the rotational speed is modulated based on wind speed measurements to maintain the TSR near its optimal value.

The utilization of multiple fidelity levels in this study allows for a pragmatic balance between computational cost

Table 2 VAWT operational settings for the high-fidelity method (LBM)

Parameter	Straight & Helical	Troposkien
Tip speed ratio (TSR)	3.3	3.3
Rotations per minute (RPM)	550.71	366.01
Chord-based Reynolds number (Re_c)	1.73×10^5	1.73×10^5

and accuracy. To keep computational costs low for this investigation, the high-fidelity LBM is employed only at TSR = 3.3. Additionally, taking advantage of faster computations for the mid-fidelity method, it is applied across a TSR range of 1 to 7 which will allow exploring a wide range of operating conditions. This is anticipated to provide comprehensive insights into VAWT fluid dynamic interactions arising from different blade shapes adopted.

For the high-fidelity LBM, the freestream Mach number (M) is set at 0.026 and all considered operational conditions in this study have Re_c values below 4×10^5 . The freestream turbulence intensity (I_t) and turbulence length scale (L_t) are both set to 0.1% and 1 mm, respectively. However, based on a prior investigation by Casalino et al. [26], it is anticipated that these parameters will not exert a significant influence on the evolution of the unsteady flow field.

The current LBM setup and the grid used have been adopted from a previous study by Shubham et al. [12], in which the setup has already been tested for grid convergence. The values of y^+ and voxels per chord for the grid used are 33.3 and 2.67×10^2 , respectively. The y^+ value is a dimensionless parameter that represents the distance of the first cell centre from the computational domain's wall in the wall-normal direction. In this study, it is computed based on the average velocity experienced by the blade at the mid-span location over a single rotation. On the other hand, the voxels per chord denote the number of grid cells along the blade's chord direction.

The smallest voxel size corresponding to the grid used is 0.321 mm, for all three VAWT configurations. For the 3-bladed VAWT, the number of fine equivalent voxels in the computational domain amounts to 30.94 million, 57.9 million and 89.9 million for straight, helical and troposkien VAWT, respectively. These fine equivalent voxels are obtained by multiplying the number of voxels by the time stepping rate, which is directly proportional to the mesh resolution level. It is worth noting that doubling the voxel size leads to a reduction in computational cost by half, as the time step is also doubled. The computational effort, expressed in CPU hours, required to simulate 12 rotor rotations (1.31 s for straight and helical, 1.97 s for troposkien) amounts to 2.01e04 for straight-bladed, 4.88e04 for helical-bladed and 9.84e04 for troposkien VAWT. These simulations were performed on a Linux workstation equipped with an AMD Ryzen Threadripper 3990X Gen3 64 Core 128GB DDR4 3GHz platform. The physical time step for the grid used corresponds to a Courant-Friedrichs-Lewy (CFL) number of 1 in the finest VR level, resulting in time step values of 1.51×10^{-6} s for straight and helical and 3.05×10^{-6} s for troposkien.

Next, for the mid-fidelity LLFVW simulations conducted using QBlade, the setup parameters are summarized in Table 3. The simulations utilized a blade panel discretization of 31, while the azimuthal timestep was adjusted proportionally to the TSR value to ensure that the resulting mesh formed by the trailing and shed vortices in the wake of the turbine maintained an aspect ratio no greater than 1.5:1. A full wake length spanning 12 rotations is employed, with a vortex time offset of 1e-4 seconds.

Table 3 Simulation parameters used for the LLFVW method

Parameters	LLFVW
Freestream velocity V_∞	9 m/s
Density	1.225 kg/m ³
Kinematic viscosity	1.65 e-5 m ² /s
Blade discretization	31 (cosine)
Azimuthal discretization	3 deg
Full wake length	12
Vortex time offset	1 e-4 sec
Turbulent vortex viscosity	100

IV. Results and Discussion

A. Temporal Convergence study and Validation

Temporal convergence characteristics of the thrust coefficient (C_T) and the torque coefficient (C_Q) for two distinct VAWT configuration, namely straight and helical, is shown in Figure 3. The reported values in the figures are representative of the overall rotor, comprising all blades in a rotor. The corresponding uncertainty values (u) are calculated as a percentage of the standard deviation of thrust and torque values averaged over a complete rotation. These uncertainty values reflect the degree of uncertainty or variability in the computed thrust and torque coefficients over time due to the inherent unsteadiness and randomness in the fluid dynamic interactions. A smaller value of u implies a higher level of confidence in the simulation outcomes, indicating that the simulation has achieved temporal convergence. All u values depicted in the figures are calculated after the 8th rotor rotation for LBM and the 15th rotor rotation for LLFVW.

It is observed that temporal convergence is achieved at the same number of rotations when comparing the straight and helical VAWT configurations for any particular variable. This signifies that the blade shape does not substantially influence the unsteady aerodynamic loading (since thrust and torque directly stem from the blade forces). A perceptible difference in the required number of rotations for convergence between thrust and torque values is evident when utilizing either of the two numerical methods. Specifically, pertaining to the C_T values, convergence is accomplished after roughly 5 rotor rotations for the LBM simulations and 10 rotor rotations for the LLFVW simulations. Conversely, for the C_Q values, temporal convergence necessitates approximately 7 rotor rotations for the LBM and 13 rotor rotations for the LLFVW results. Therefore, C_T exhibits convergence at a smaller number of rotations, as also exemplified by the low uncertainty values (u), unlike the C_Q s. This observation is consistent with preceding investigations on VAWTs operating at low Reynolds numbers [12, 45], thus further validating the current study outcomes.

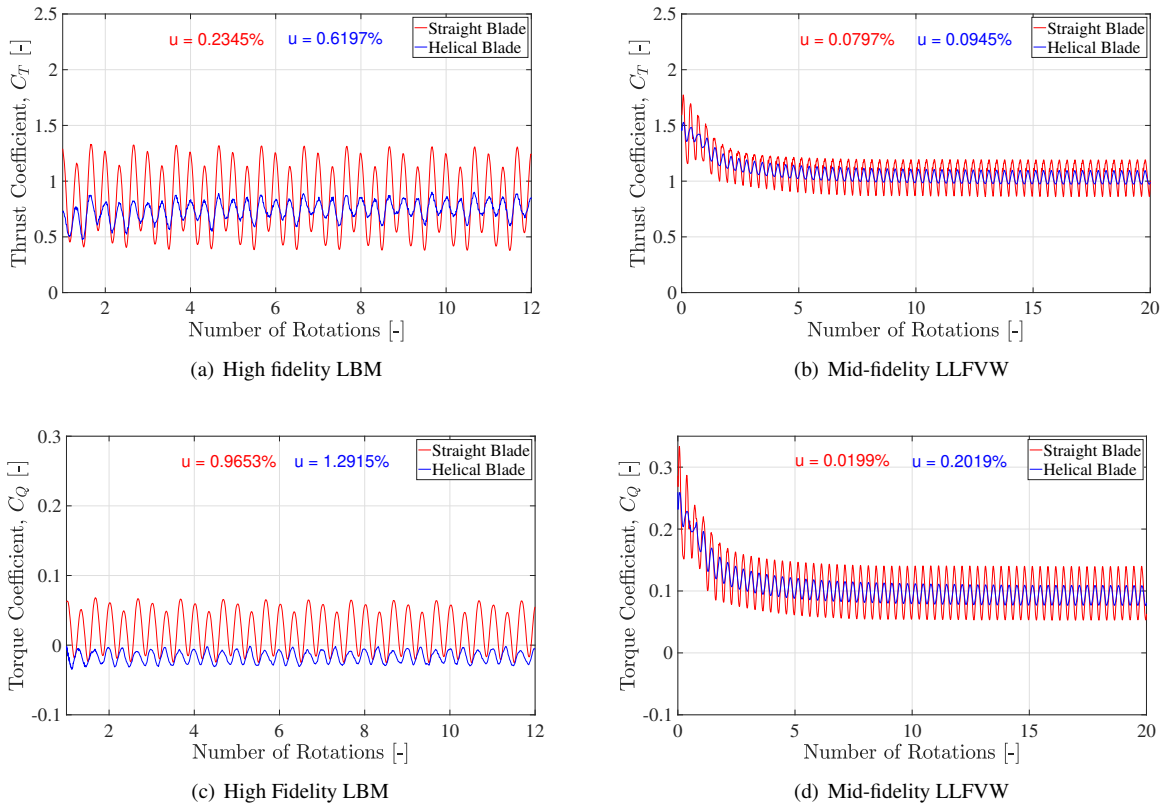


Fig. 3 Statistical Temporal Convergence study for VAWT thrust coefficient C_T and torque coefficient C_Q using LBM in PowerFlow and LLFVW in QBlade

The temporal convergence of unsteady pressure data for straight and helical configurations is investigated using the high-fidelity LBM in Figure 4. The data is collected at a specific location in the mid-span plane of rotation of the

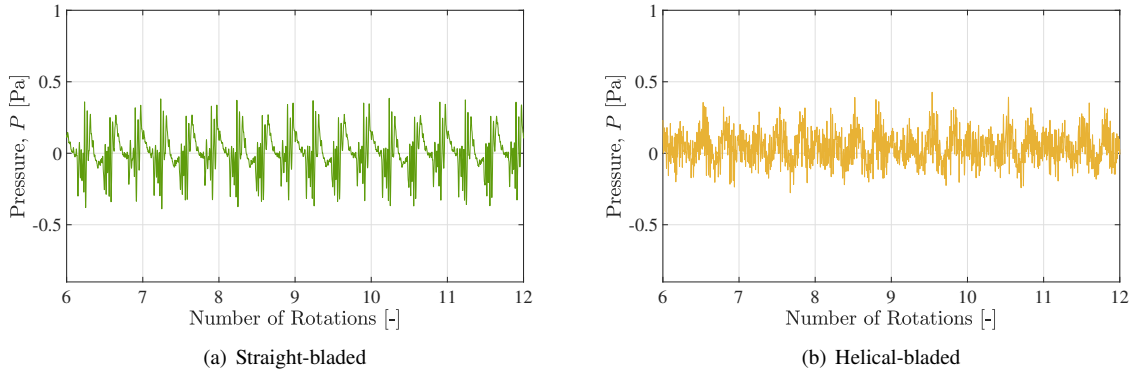


Fig. 4 Statistical temporal convergence study for unsteady pressure data at $\text{TSR} = 3.3$ at location $(X,Y,Z)=(0,0,7D)$, using the high-fidelity LBM

blade, positioned at a lateral distance of $7D$ from the centre of the VAWT $(0,0,7D)$. After six rotor rotations, pressure data are recorded for both configurations, and the results indicate that temporal convergence is achieved after the 10th rotation for both the straight and helical configurations. Therefore, keeping in mind the temporal convergence of both aerodynamics and aeroacoustics, all subsequent analysis in this study focuses on data obtained after the 10th rotation using the high-fidelity LBM and the 20th rotation using the mid-fidelity LLFVW method. Notably, the fluctuations in pressure decreases for the helical VAWT as compared to the straight VAWT, although the reduction is not substantial. Furthermore, the straight-bladed configuration exhibits noise which is more tonal in nature, whereas the helical configuration produces noise with a more broadband nature.

Figure 5 shows the variation of C_P values for a range of TSR from 1 - 8, obtained using the mid-fidelity LLFVW method, for a 1-bladed Darrieus VAWT. High-fidelity LBM result for $\text{TSR} = 3.3$ is also included in the figure, and a comparison is made with the reference results of Balduzzi et al. [11]. The reference dataset consists of the mid-fidelity LLFVW method and the high-fidelity 3D CFD method, utilizing the compressible formulation of the Reynolds-averaged Navier-Stokes (RANS) equations, only for a TSR of 3.3. A good agreement can be seen in all the results, with the values falling within 5 – 10% of the reference results. A slight deviation of C_P values from the reference results can be seen at low TSR which suggests that the airfoil extrapolation and dynamic stall model used in the mid-fidelity needs further investigation. However, the overall results show very good numerical validation, and hence the computational setup is good enough to provide sufficient analysis of the VAWT fluid dynamic interactions.

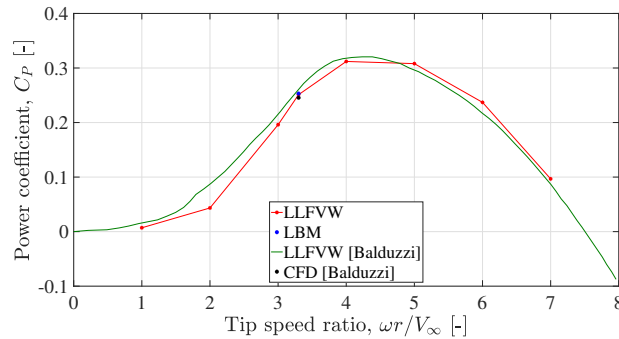


Fig. 5 C_P values for a range of TSR using QBlade and for $\text{TSR} = 3.3$ using PowerFLOW for the 1-bladed Darrieus VAWT; comparison is made with results from Balduzzi[11]

B. Aerodynamics

Figure 6 shows the variation of average power coefficient C_P and thrust coefficient C_T with TSR, comparing the values for three different blade shapes used in this study, namely straight, troposkein and helical. The troposkein rotor

exhibits a smooth and large range of operation, while the straight and helical-bladed rotors display a distinct peak in their power and thrust coefficients. Remarkably, the C_P and C_T values for the helical and straight VAWTs exhibit a coincidental similarity in their variations with changing tip speed ratio (TSR), with only negligible differences discerned between the two configurations. The maximum efficiency for all three rotor designs occurs within the TSR range of 3-4 (optimal TSR), beyond which a gradual decline in performance is observed. It can be observed that at a lower TSR, the straight and helical configuration attains a greater value of C_P than the troposkein indicating that the self-starting of the VAWT, which happens at low TSR will be better for VAWT with straight or helical blade designs. Moreover, at a higher TSR, troposkein is observed to provide a greater value of power than the other two configurations.

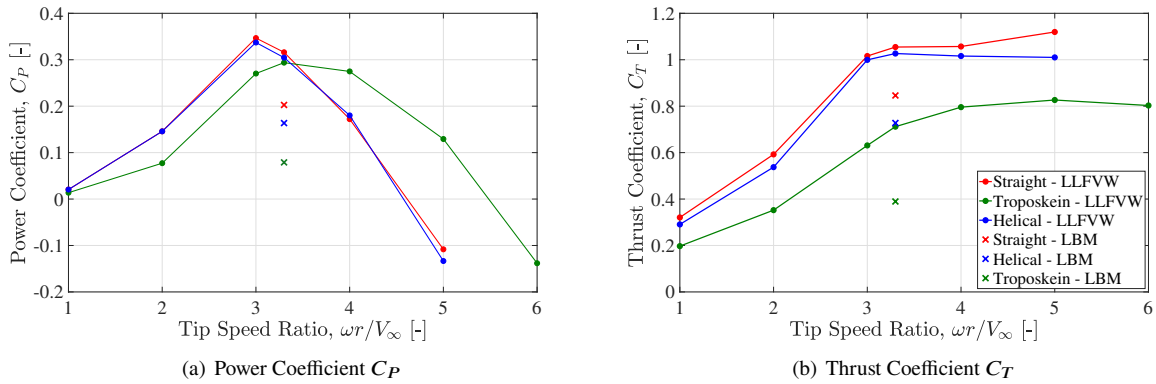


Fig. 6 Variation of C_P and C_T with tip speed ratio (TSR) obtained for different blade designs, using mid-fidelity LLFVW (line plot) and high fidelity LBM at TSR = 3.3 (single cross)

As the rotor extracts more energy from the incoming flow, it creates a greater blockage. This is characterised by the induction factor. The induction factor refers to the ratio of the difference between the freestream wind velocity and the actual wind velocity experienced by the blades with the freestream wind velocity. In other words, it is the factor by which the VAWT offers blockage to the incoming flow and denotes the fractional decrease in wind speed due to the presence of the VAWT. The induction factor has a very strong dependence on the design of the rotor blades and is influenced by both TSR and rotor solidity.

An increase in the induction factor has two effects on the performance of the VAWT:

- Reduces the free-stream velocity in both the upwind and the downwind half of the rotor (more decrease for the latter), resulting in an effective increase in TSR, which consequently reduces the blade angle of attack.
- Increases the flow blockage which deflects the incoming flow away from the upwind half of the rotor and affects the downstream VAWT flowfield.

When the TSR increases, there is an increase in the induction factor, which means that a larger fraction of the wind's energy is extracted by the turbine. Initially, C_P increases up to the optimal TSR value due to an increase in blade rotational speed and a decrease in dynamic and deep stall phenomena. As TSR further increases, C_P decreases due to a decrease in wind velocity experienced by the blades (very high induction factor) and a subsequent decrease in blade angle of attack in both the upwind and downwind halves of rotation.

In the present study, involving three different configurations (Straight, Troposkein and Helical), though the rotor solidity for all three configurations is the same (it has to be noted that the solidity of troposkein varies radially; however the solidity at the equator for troposkein is equal to the solidity of other two configurations), it can be observed that the straight and helical configurations reach their peak power coefficient at lower TSR compared to the troposkein configuration. This leads to the conclusion that the former provides much more blockage to the incoming flow (increased induction factor) than the troposkein configuration. This increased blockage is a consequence of different blade designs. Additionally, at high TSR values, the higher induction factor of a rotor causes the power to drop even further, which can be observed by the sharper gradient of C_P for the straight and helical configurations in Figure 6 (a).

At TSR = 3.3, results are compared between the high-fidelity LBM and mid-fidelity LLFVW, and a significant difference in the results is obtained between both of these methods. The difference in C_P values is the least (0.1134) for the straight configuration, followed by the helical (0.1409) and troposkein (0.2147). A similar trend is observed with the results of thrust coefficient, which suggests that the LLFVW method fails to capture the complex 3D effects in the flow

and the force fields as effectively as the LBM. This inconsistency is not unexpected, since the basis of fluid modelling of both methods is different. Even though there are differences observed between the results of the two numerical methods, the trend of the C_P and C_T values obtained by both the numerical methods for the three configurations remain the same. Contrary to the initial expectations and the prevailing literature [46, 47], mid-fidelity results obtained from the QBlade produced minimal variation in results between the straight and helical configuration as seen in Figure 6.

Figure 7 illustrates the variation of C_Q and C_T of the overall rotor over a complete single rotation as obtained using the high-fidelity and mid-fidelity simulations at TSR = 3.3. The figure also presents the average value over a complete rotation which corresponds to values presented in Figure 6. It can be inferred from the figure that the helical rotor has a smooth variation of torque and thrust coefficient as compared to the troposkein and straight configuration, where the straight configuration has the highest amplitude of variation of C_Q and C_T over a single rotation.

A helical blade can be divided into three sections; a leading section, a mid-section and the trailing section. The leading section enters any quartile azimuthal first followed by the mid-section and trailing section while the turbine is in rotation. The mid-section of the helical blade contributes greatest to the performance of the overall rotor than the other two sections [48]. The mid-section of the helical configuration is distributed over a greater range of azimuthal angles, and hence the overall rotor loading is distributed over a wide range of azimuthal angles, making the variation in blade loading smooth.

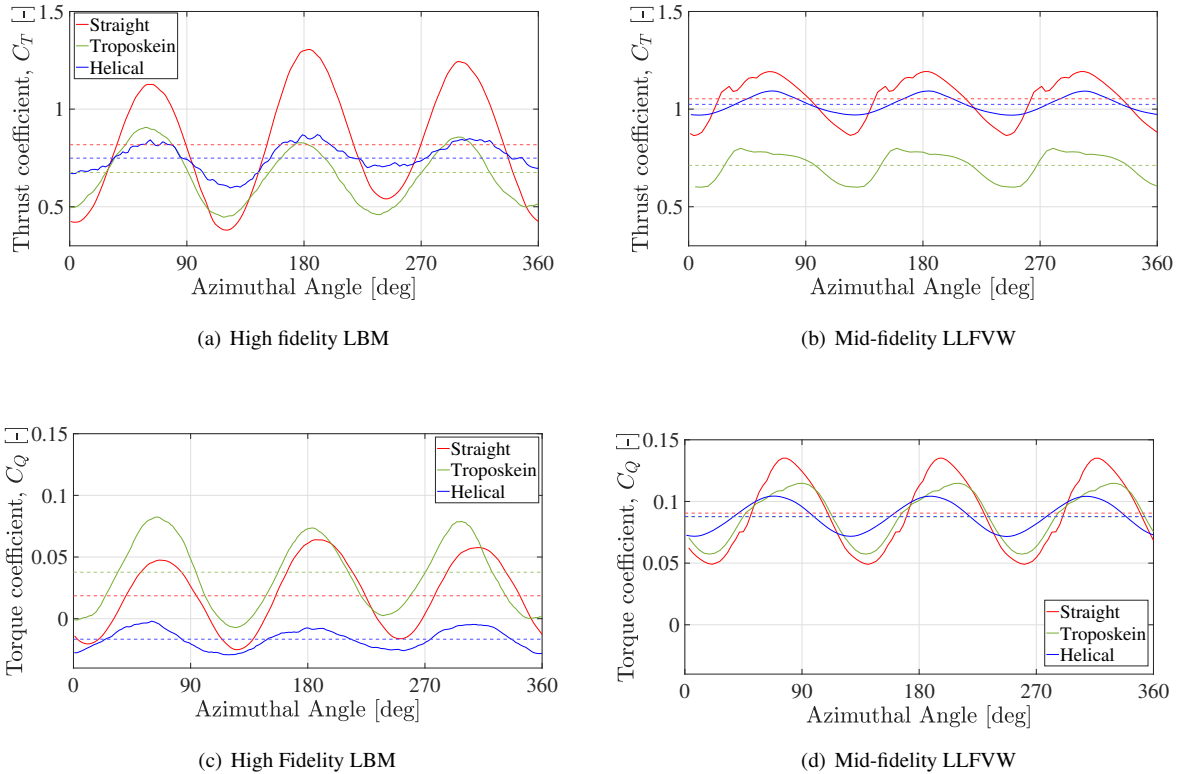


Fig. 7 Variation of Torque Coefficient C_Q and Thrust Coefficient C_T for the overall rotor over a complete single rotation using the high-fidelity LBM and mid-fidelity LLFVW at TSR = 3.3

Figure 8 depicts the variation of the C_Q and C_T for a single blade over 360° azimuthal angle at TSR = 3.3, as predicted by high-fidelity LBM and mid-fidelity LLFVW simulations for the three VAWT configurations. The average values in a single rotation are also shown in the figures. Both methods indicate that the straight blade generates the highest average thrust. The LBM predicts the thrust of the straight blade to be maximum in the upwind region but relatively constant and lowest amongst the three blade shapes in the downwind region. The LLFVW method agrees well with the LBM for the straight blade, except in the downwind region where all three blade shapes exhibit similar thrust in the case of the former.

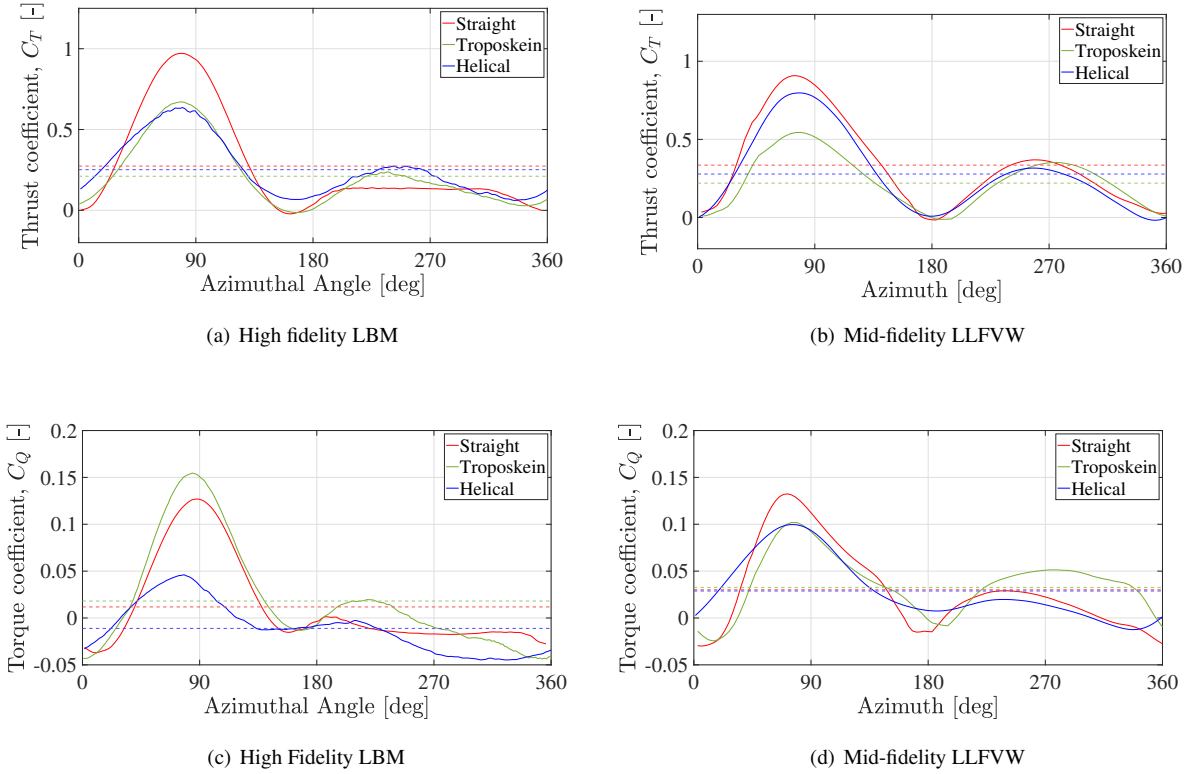


Fig. 8 Variation of Torque Coefficient C_Q and Thrust Coefficient C_T for the single blade over a complete single rotation using the high-fidelity LBM and mid-fidelity LLFVW at $TSR = 3.3$

For the troposkein and helical blades, differences can be seen between the LBM and LLFVW predictions. The LBM shows comparable thrust for these two blade shapes upwind, whereas, in the downwind part, the helical blade outperforms troposkein. The mean thrust of helical VAWT approaches that of the straight VAWT. In contrast, the LLFVW results suggest the helical blade generates higher thrust than the troposkein blade upwind, and vice versa in the downwind part of the rotation. Regarding torque, the LBM predicts that the troposkein blade produces maximum torque both upwind and downwind, followed by the straight and helical blades. The LLFVW method indicates that the straight blade yields the highest torque upwind, while the troposkein blade surpasses the other two in the downwind part and in the mean torque value. Notably, the LBM shows substantially lower torque for the helical as compared to the straight blade, dissimilar to the LLFVW outcomes. Overall, the results suggest that LLFVW does not capture the relevant physics, particularly in the downwind region where complex 3D flow dynamics like blade-wake and blade-vortex interactions are significant.

These variations of the C_T and C_Q values for a single blade over a complete rotation are in alignment with the variation of C_T and C_Q values of the overall rotor as seen in Figure 7. While some consistencies emerge, discrepancies between the LBM and LLFVW methods are apparent for all blade shapes. This discrepancy may be attributable to the XFOIL polar data (c_l and c_d versus angle of attack α) utilized in the analytical LLFVW calculations, which impact the predicted blade angle of attack and induced velocity. To enhance model fidelity, future work could explore modifying the XFOIL polars through empirical corrections. Another potential avenue is substituting experimentally-derived polars encompassing the full 360° angle of attack range, as obtained from wind tunnel testing [49]. Employing such refinements to the airfoil data could lead to improved representation of the complex three-dimensional flowfield and blade-wake interactions.

To gain a deeper understanding of the impact of the blade-wake and blade-vortex interaction on overall rotor performance, Figure 9 provides insight into instantaneous vortices in the downstream part of the VAWT flowfield using iso-surfaces of the λ_2 criterion for $TSR = 3.3$. The convective motion of the large vortex structures (shed and

trailing tip vortices) downstream is accompanied by wake expansion and progressive disintegration into smaller-scale structures caused by flow instabilities and spatial modulation, which eventually dissipate and mix with the ambient fluid [50, 51]. Across the three VAWT configurations, a discernible variation arises in the sizes of primary vortex structures, encompassing larger coherent vortices and smaller incoherent ones. Specifically, vortex density is the lowest for straight and highest for helical VAWT, which means the latter experiences a greater blade-vortex interaction (BVI) compared to the former at $TSR = 3.3$. This difference in BVI correlates with the level of three-dimensional complexity inherent to each blade design. The twisted helical shape exhibits the most substantial spanwise variation in angle of attack and associated flow curvature. This non-uniformity introduced across the blade length likely promotes the roll-up of vorticity into larger coherent structures.

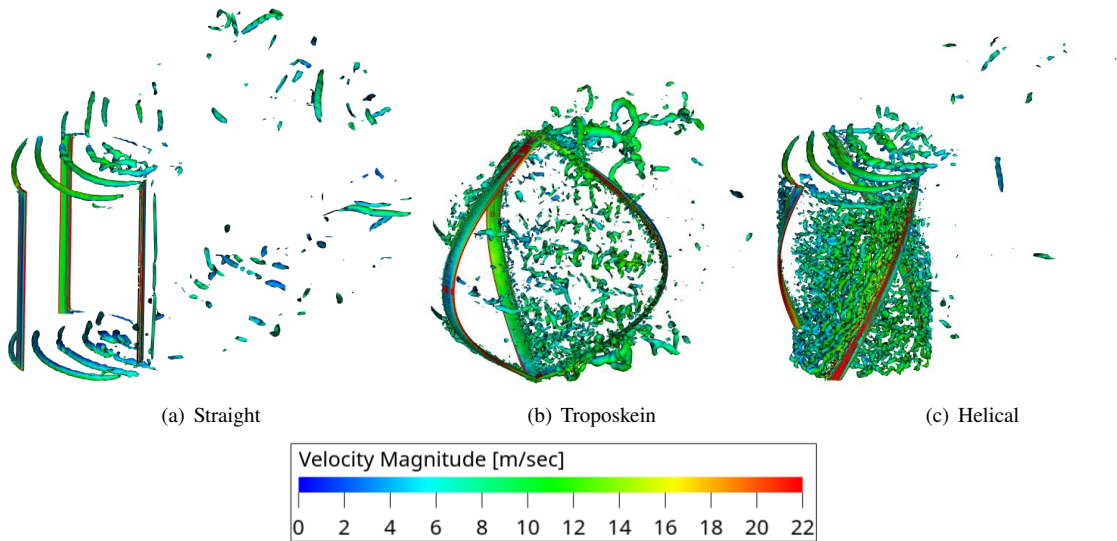


Fig. 9 Instantaneous 3D flowfield using iso-surfaces of the λ_2 criterion for vortices visualization, using high-fidelity LBM, at $TSR = 3.3$

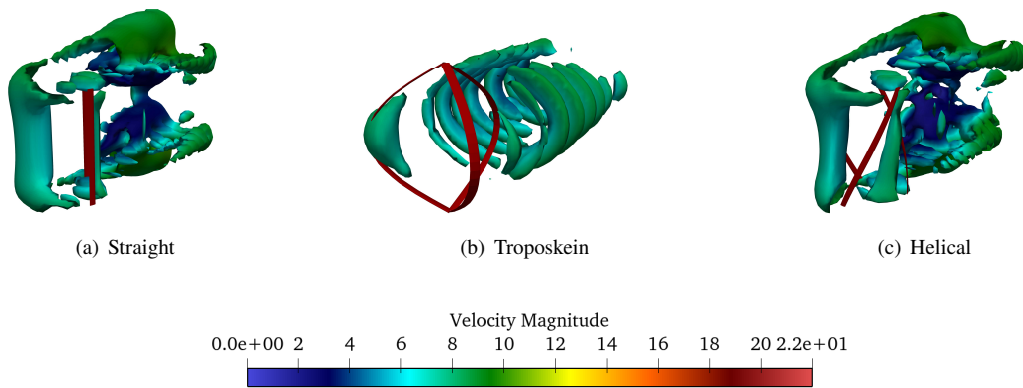


Fig. 10 Instantaneous 3D flowfield using iso-surfaces of the Q criterion for vortices visualization, using mid-fidelity LLFVW, at $TSR = 3.3$

The coherent tip vortices shed from the tip of each blade are particularly significant, especially when comparing the three configurations. These tip vortices convect downstream and create a spiral flow pattern, also known as a "vortex ring," that wraps around the turbine's axis [12]. The vortex ring is not visible in troposkein VAWT, instead a single vortex strand is visible shed from the top and bottom of the VAWT. This minimizes the tip vortex effect on the troposkein blade loading as compared to straight and helical and this causes lower performance loss and higher power output at

high TSRs, for the former, as seen in Figure 6 (a). Change in the blade shape directly influences the loading distribution along the chordwise and spanwise direction, leading to the difference in the vortex strength and density in the wake of three configurations, and consequently influencing the downwind performance of the blade as seen in Figure 8.

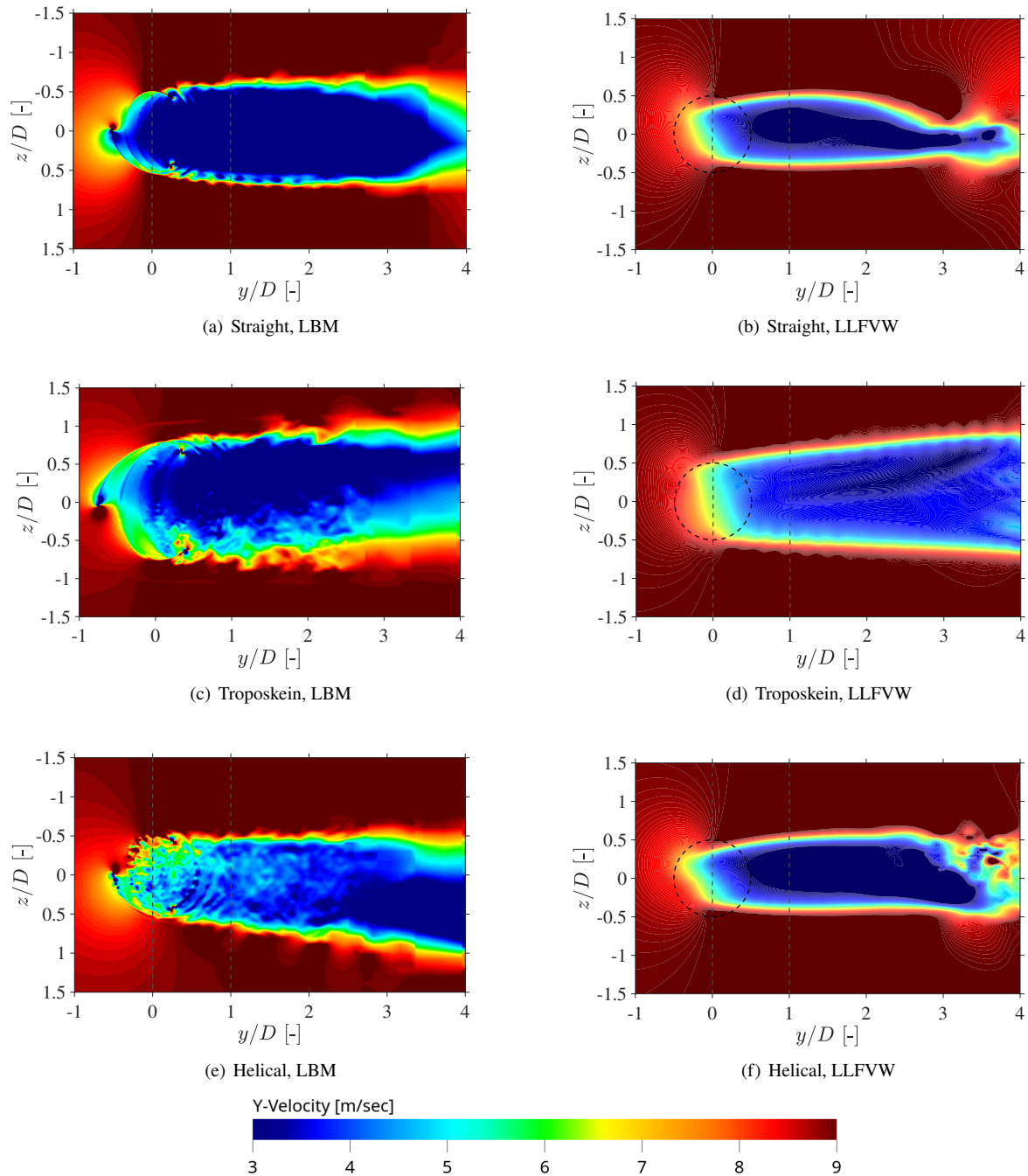


Fig. 11 Instantaneous streamwise velocity contours in the VAWT wake on a 2D plane located at the blade mid-span location, using both LBM and LLFVW methods at TSR = 3.3

Figure 10 shows instantaneous 3D vortices using the mid-fidelity LLFVW approach. Contrary to high-fidelity results, the mid-fidelity analysis was unable to discern a notable distinction in BVI between the three configurations as evident from similar vortex density in the flowfield of all configurations. This is one of the reasons straight and helical performance is similar as predicted by the mid-fidelity method, as seen in Figure 6 (a) and (b). These outcomes conclude

that the LLFVW method fails to capture the effect of blade shape between straight and helical when the solidity of the rotor is the same.

Figure 11 displays the instantaneous streamwise velocity contours in the VAWT wake on a 2D plane located at the blade mid-span location, using both LBM and LLFVW methods for $TSR = 3.3$. It can be observed that the downstream wake is strongest for straight, followed by troposkein and then helical configuration. This also shows the variation in flow blockage and induction factor exhibited by different blade shapes, reducing the velocity induced at the upstream blades. This effect is further magnified when the blades reach the downwind part of the rotation. Consequently, the aerodynamic performance of downstream blades is inferior to that of the upstream blades, as evidenced by the results of thrust and torque presented in Figures 8 and 7. Both LBM and LLFVW methods capture the reduction in streamwise velocities across the three configurations, although LLFVW predicts lower velocities compared to LBM for the straight and helical configurations.

The strength of the downstream wake proportionately increases with the strength of the force distribution on an airfoil or blade, (as predicted by LBM, the straight configuration having the strongest downstream wake, has the highest thrust in a single rotation) which is consistent with the results of the overall rotor thrust and single blade thrust shown in Figure 7 and Figure 8, respectively. The prediction of higher rotor thrust values by LLFVW relative to LBM leads to lower prediction of streamwise velocities in the wake of the former. Moreover, the 2D vortex structures illustrated in Figure 11 for LBM are more prominent than those for LLFVW. These structures are indicative of shed vortices, as demonstrated by the 3D view presented in Figure 9, and the differences in vortex modelling approaches suggest that LBM is more effective in capturing the blade vortex interaction.

C. Aeroacoustics

Figure 12 illustrates the raw unsteady pressure data generated by the three different VAWT configurations (Straight, Troposkein and Helical) obtained at two different locations, one situated in the plane of rotation at $(0,0,7D)$ in the cross-streamwise/lateral direction, and another situated out of plane at $(4D,0,7D)$ just above the first location. The data is reported for a single rotor rotation obtained using high-fidelity LBM. The findings reveal that the amplitude of pressure fluctuations at the out-of-plane location is lower as compared to the in-plane location across all blade configurations. Evaluating the blade geometries, the troposkein exhibited the highest fluctuation levels followed by the straight and helical shapes at both measurement locations. This trend aligns with the variation of torque values as shown in Figures 8 and 7 over a complete single rotation obtained from the LBM model.

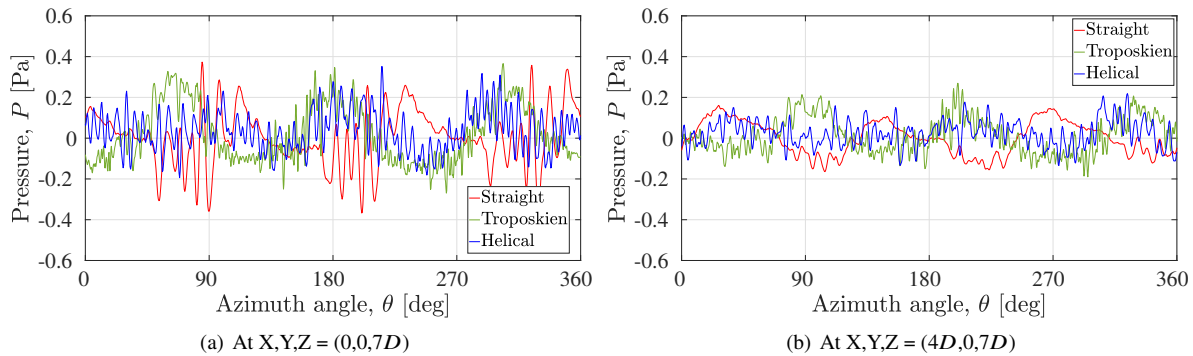


Fig. 12 Raw unsteady pressure data for three different VAWT configurations using the high-fidelity LBM at two different locations at $TSR = 3.3$; the data presented is sampled from all the blades

Figure 13 reports the sound pressure level (SPL) values in dB/Hz over a frequency range of 20-2000 Hz obtained using high-fidelity LBM, at the two observer locations considered in this study. The noise spectra reveal complementary characteristics. Broadly, noise levels are lower for the out-of-plane location across all frequencies. At lower frequencies (20-30 Hz), troposkein has the highest noise level, followed by straight and then helical geometry. The continuous smooth azimuthal blade loading for the helical shape is postulated to reduce pressure fluctuations and mitigate noise emissions. However, at higher frequencies (500-2000 Hz), both troposkein and helical produce more noise than the straight blade. From Figure 9, it is clear that helical and troposkein blades have much higher BVI/BWI than the straight blade, which increases the unsteady blade loading causing an increase in high-frequency pressure fluctuations, as can be

seen in Figure 12 (b).

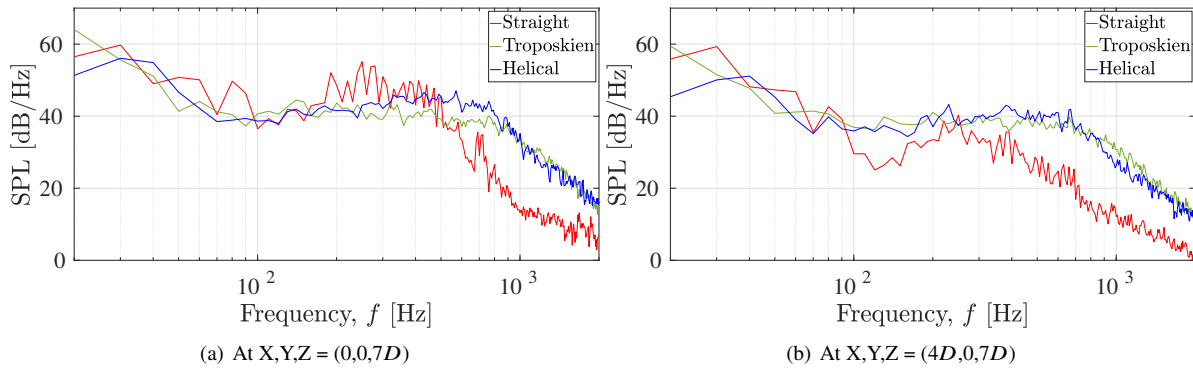


Fig. 13 Sound Pressure Level (SPL) spectra for three different VAWT configurations using the high-fidelity LBM at two different locations at TSR = 3.3; the data presented is sampled from all the blades

V. Conclusion

This research presents a comprehensive investigation into the influence of blade shape on the aerodynamic and aeroacoustic characteristics of vertical axis wind turbines (VAWTs) employing a Darrieus rotor. The aims of this work are twofold: to enable the development of a multi-fidelity simulation framework for VAWT force and flow field analysis, and to examine the effects of blade design on VAWT performance. High-fidelity aerodynamic simulations are conducted using the Lattice Boltzmann Method (LBM) approach, with far-field noise calculations performed via the Ffowcs Williams and Hawkins (FW-H) method. Additionally, mid-fidelity simulations utilizing the Lifting Line Free Vortex Wake (LLFVW) technique are implemented. The study focuses on assessing the impact of varying blade shapes on thrust and power performance, alongside far-field noise emissions. Furthermore, results obtained from the 3D force and flow fields using the mid- and high-fidelity methods are compared, aiming to identify potential discrepancies in the modelling of fluid dynamic interactions that may manifest as differences in the resultant data.

It is observed that the number of rotations required for attaining statistical temporal convergence is invariant between any blade shape of the VAWT. The thrust coefficients converge within just 5 rotor revolutions with reduced uncertainty whereas 10 rotations are necessary for torque coefficient convergence, as discerned from the high-fidelity LBM simulations. The comparative analysis of the mid-fidelity LLFVW and the high-fidelity LBM results shows their respective efficiency in capturing the influence of the blade shape on flow physics. Straight blade generates the most power, followed by helical and troposkein, as both LBM and LLFVW methods predicted. However, the LLFVW method predicted the performance of the helical configuration to be higher than that predicted by the LBM method. The LLFVW results consistently estimate higher thrust and torque values across the upwind and downwind parts of rotation relative to the LBM. Troposkein and helical VAWTs exhibit a higher density of vortex structures in the downstream flowfield, as compared to the straight VAWT. This is likely a result of spanwise variation in blade loading and angle of attack in the former, which is not present in the latter.

This pattern is also reflected when calculating the mean thrust (higher by 21%) and torque values (higher by 23%) for all VAWT configurations. However, this relative percentage of estimating higher values is reduced when calculating for a single blade of the VAWT configuration in a complete rotation, to 10% for the mean thrust and 17% for the mean torque. This implies a potential limitation of the LLFVW method in adequately capturing the intricate 3D effects inherent in the flow and force fields of the VAWT, particularly when considering variations in blade shapes. Consequently, the LLFVW method predicts a higher integral thrust and power for the entire rotor than the LBM. The LLFVW method, due to increased loading on the blades, predicts lower streamwise wake velocities, resulting in a more pronounced wake than that predicted by LBM. These findings underscore the importance of judiciously selecting an appropriate fidelity level, especially when intricate three-dimensional fluid dynamic interactions characterize a rotor setup. Additionally, these observations present an opportunity for enhancing predictive accuracy by refining the mid-fidelity method.

The present study also compares the aeroacoustic properties across the three VAWT configurations, using only the high-fidelity LBM. At lower frequencies, troposkein has the highest noise level, followed by straight and then helical geometries, which follow a similar trend as the mean torque values in a single rotation. However, at higher frequencies,

both troposkein and helical blades produced more noise than the straight blade due to higher BVI/BWI exhibited by the former.

Future studies should explore new designs, such as a hybrid of troposkein and helical, to obtain a wider range of operation (like in troposkein) and smoother blade loading and lower noise (like in helical). The airfoil polar data within the LLFVW framework can be refined, and empirical modifications can be made to reflect blade-wake and blade-vortex interactions more accurately, aligning with experimental results. Noise sources should be investigated to better the effect of different blade shapes on VAWT aeroacoustics, using the beamforming method. The current study can be extended to include other numerical methods such as the Actuator Cylinder (AC) model, Vortex Panel Method (VPM), Non-linear Vortex Lattice Method (NVLM), and Reformulated Vortex Particle Method (RVPM). An extension of the current study will explore such topics along with real-life experimental results obtained from a helical-bladed small-scale VAWT installed at Nottingham Trent University, UK.

VI. Acknowledgments

For the part of high-fidelity simulations, this project has received funding from the European Union's Horizon 2020 Marie Curie zEPHYR research and innovation programme under grant agreement No EC grant 860101 (<https://www.h2020-zephyr.eu/>). Nottingham Trent University has received sponsorship from 3DS Simulia for the commercial software PowerFLOW.

References

- [1] Desa, U. N., "World urbanization prospects: the 2018 revision, key facts," *New York: NY. Available online at: <https://population.un.org/wup/Publications/>* (Accessed December 20, 2018), 2018.
- [2] Van Kuik, G., Peinke, J., Nijssen, R., Lekou, D., Mann, J., Sørensen, J. N., Ferreira, C., van Wingerden, J.-W., Schlipf, D., Gebraad, P., et al., "Long-term research challenges in wind energy—a research agenda by the European Academy of Wind Energy," *Wind energy science*, Vol. 1, No. 1, 2016, pp. 1–39.
- [3] Quintero Pulido, D. F., Ten Kortenaar, M. V., Hurink, J. L., and Smit, G. J., "The role of off-grid houses in the energy transition with a case study in the Netherlands," *Energies*, Vol. 12, No. 10, 2019, p. 2033.
- [4] Dabiri, J. O., "Potential order-of-magnitude enhancement of wind farm power density via counter-rotating vertical-axis wind turbine arrays," *Journal of renewable and sustainable energy*, Vol. 3, No. 4, 2011, p. 043104.
- [5] Shubham, S., Naik, K., Sachar, S., and Ianakiev, A., "Performance analysis of low Reynolds number vertical axis wind turbines using low-fidelity and mid-fidelity methods and wind conditions in the city of Nottingham," *Energy*, Vol. 279, 2023, p. 127904.
- [6] Shubham, S., Ianakiev, A., and Wright, N., "Review of standalone small-scale Darrieus wind turbines - a Nottingham case study," *17th EAWE PhD Seminar on Wind Energy*, 2021.
- [7] Kumar, R., Raahemifar, K., and Fung, A. S., "A critical review of vertical axis wind turbines for urban applications," *Renewable and Sustainable Energy Reviews*, Vol. 89, 2018, pp. 281–291.
- [8] AR Sengupta, R., A.Biswas, "Comparison of low wind speed aerodynamics of unsymmetrical blade H-Darrieus rotors-blade camber and curvature signatures for performance improvement," 2019.
- [9] Mohammad, M., "Performance investigation of H-rotor Darrieus turbine with new airfoil shapes," 2012.
- [10] J. Chen, H. X. e. a., P. Liu, "A detailed investigation of a novel vertical axis Darrieus wind rotor with two sets of blades," 2017.
- [11] Balduzzi, F., Marten, D., Bianchini, A., Drofelnik, J., Ferrari, L., Campobasso, M. S., Pechlivanoglou, G., Nayeri, C. N., Ferrara, G., and Paschereit, C. O., "Three-dimensional aerodynamic analysis of a Darrieus wind turbine blade using computational fluid dynamics and lifting line theory," *Journal of Engineering for Gas Turbines and Power*, Vol. 140, No. 2, 2018.
- [12] Shubham, S., Wright, N., Avallone, F., and Ianakiev, A., "Aerodynamic and aeroacoustic investigation of vertical axis wind turbines with different number of blades using mid-fidelity and high-fidelity methods," *AIAA AVIATION 2023 Forum*, 2023, p. 3642.
- [13] Shubham, S., Avallone, F., Brandetti, L., Wright, N., and Ianakiev, A., "Effect of struts and central tower on aerodynamics and aeroacoustics of vertical axis wind turbines using mid-fidelity and high-fidelity methods," *AIAA SciTech Forum*, 2024.

- [14] Shubham, S., Kipouros, T., Dash, S., and Ianakiev, A., “Uncertainty propagation and management of mixed uncertainties for multi-fidelity multi-disciplinary analysis of propeller with different blade sweep,” *AIAA SciTech Forum*, 2024.
- [15] Marten, D., Bianchini, A., Pechlivanoglou, G., Balduzzi, F., Nayeri, C. N., Ferrara, G., Paschereit, C. O., and Ferrari, L., “Effects of airfoil’s polar data in the stall region on the estimation of Darrieus wind turbine performance,” *Journal of Engineering for Gas Turbines and Power*, Vol. 139, No. 2, 2017.
- [16] Van Garrel, A., “Development of a wind turbine aerodynamics simulation module,” 2003.
- [17] Marten, D., “QBlade Guidelines v0. 95,” *Technical University of Berlin, Berlin, Germany*, 2016.
- [18] Marten, D., Lennie, M., Pechlivanoglou, G., Nayeri, C. N., and Paschereit, C. O., “Implementation, optimization, and validation of a nonlinear lifting line-free vortex wake module within the wind turbine simulation code qblade,” *Journal of Engineering for Gas Turbines and Power*, Vol. 138, No. 7, 2016.
- [19] Marten, D., Pechlivanoglou, G., Navid Nayeri, C., and Oliver Paschereit, C., “Nonlinear lifting line theory applied to vertical axis wind turbines: Development of a practical design tool,” *Journal of Fluids Engineering*, Vol. 140, No. 2, 2018.
- [20] Bergami, L., and Gaunaa, M., “ATEFlap Aerodynamic Model, a dynamic stall model including the effects of trailing edge flap deflection,” 2012.
- [21] Wendler, J., Marten, D., Pechlivanoglou, G., Nayeri, C. N., and Paschereit, C. O., “An unsteady aerodynamics model for lifting line free vortex wake simulations of hawt and vawt in qblade,” *Turbo Expo: Power for Land, Sea, and Air*, Vol. 49873, American Society of Mechanical Engineers, 2016, p. V009T46A011.
- [22] Gourdain, N., Jardin, T., Serre, R., Prothin, S., and Moschetta, J.-M., “Application of a lattice Boltzmann method to some challenges related to micro-air vehicles,” *International Journal of Micro Air Vehicles*, Vol. 10, No. 3, 2018, pp. 285–299.
- [23] Shubham, S., Avallone, F., Grande, E., and Casalino, D., “Computational Aeroacoustic Investigation of Co-rotating rotors for Urban Air Mobility,” *Delft International Conference on Urban Air-Mobility*, 2021.
- [24] Shubham, S., “Computational Aeroacoustic Investigation of Co-rotating rotors for Urban Air Mobility,” 2020.
- [25] Avallone, F., van den Ende, L., Li, Q., Ragni, D., Casalino, D., Eitelberg, G., and Veldhuis, L., “Aerodynamic and aeroacoustic effects of swirl recovery vanes length,” *Journal of Aircraft*, Vol. 56, No. 6, 2019, pp. 2223–2235.
- [26] Casalino, D., Hazir, A., and Mann, A., “Turbofan broadband noise prediction using the lattice Boltzmann method,” *AIAA Journal*, Vol. 56, No. 2, 2018, pp. 609–628.
- [27] Nardari, C., Casalino, D., Polidoro, F., Coralic, V., Lew, P.-T., and Brodie, J., “Numerical and experimental investigation of flow confinement effects on UAV rotor noise,” *25th AIAA/CEAS Aeroacoustics Conference*, 2019, p. 2497.
- [28] Succi, S., *The lattice Boltzmann equation for fluid dynamics and beyond*, 1st ed., Clarendon Press, Oxford, 2001.
- [29] Shan, X., Yuan, X.-F., and Chen, H., “Kinetic theory representation of hydrodynamics: a way beyond the Navier–Stokes equation,” *Journal of Fluid Mechanics*, Vol. 550, 2006, pp. 413–441. <https://doi.org/10.1017/S0022112005008153>, URL http://www.journals.cambridge.org/abstract_S0022112005008153.
- [30] Chen, S., and Doolen, G., “Lattice Boltzmann method for fluid flows,” *Annual Review of Fluid Mechanics*, Vol. 30, No. 1, 1998, pp. 329–364. <https://doi.org/10.1146/annurev.fluid.30.1.329>, URL <http://www.annualreviews.org/doi/10.1146/annurev.fluid.30.1.329>.
- [31] Chen, H., Chen, S., and Matthaeus, W., “Recovery of the Navier-Stokes equations using a lattice-gas Boltzmann method,” *Physical Review A*, Vol. 45, No. 8, 1992, pp. R5339–R5342. <https://doi.org/10.1103/PhysRevA.45.R5339>, URL <https://link.aps.org/doi/10.1103/PhysRevA.45.R5339>.
- [32] Chen, H., Zhang, R., and Gopalakrishnan, P., “Lattice Boltzmann Collision Operators Enforcing Isotropy and Galilean Invariance,” 8 2015. URL <https://patents.google.com/patent/US20150356217A1/en>.
- [33] Yakhot, V., and Orszag, S., “Renormalization group analysis of turbulence. I. Basic theory,” *Journal of Scientific Computing*, Vol. 1, No. 1, 1986, pp. 3–51. <https://doi.org/10.1007/BF01061452>, URL <http://link.springer.com/10.1007/BF01061452>.
- [34] Teixeira, C., “Incorporating Turbulence Models into the Lattice-Boltzmann Method,” *International Journal of Modern Physics C*, Vol. 09, No. 08, 1998, pp. 1159–1175. <https://doi.org/10.1142/S0129183198001060>, URL <http://www.worldscientific.com/doi/abs/10.1142/S0129183198001060>.

- [35] Wilcox, D., *Turbulence modelling for CFD (Third Edition)*, DCW Industries, Incorporated, 2006.
- [36] Launder, B., and Spalding, D., “The numerical computation of turbulent flows,” *Computer Methods in Applied Mechanics and Engineering*, Vol. 3, No. 2, 1974, pp. 269–289. [https://doi.org/10.1016/0045-7825\(74\)90029-2](https://doi.org/10.1016/0045-7825(74)90029-2), URL <http://www.sciencedirect.com/science/article/pii/0045782574900292>.
- [37] Ffowcs Williams, J. E., and Hawkings, D. L., “Sound generation by turbulence and surfaces in arbitrary motion,” *Philosophical Transactions of the Royal Society of London. Series A, Mathematical and Physical Sciences*, Vol. 264, No. 1151, 1969, pp. 321–342.
- [38] Farassat, F., and Succi, G. P., “A review of propeller discrete frequency noise prediction technology with emphasis on two current methods for time domain calculations,” *Journal of Sound and Vibration*, Vol. 71, No. 3, 1980, pp. 399–419.
- [39] Brès, G., Pérot, F., and Freed, D., “Properties of the lattice Boltzmann method for acoustics,” *15th AIAA/CEAS Aeroacoustics Conference (30th AIAA Aeroacoustics Conference)*, 2009, p. 3395.
- [40] Casalino, D., “An advanced time approach for acoustic analogy predictions,” *Journal of Sound and Vibration*, Vol. 261, No. 4, 2003, pp. 583–612.
- [41] Rainbird, J. M., Bianchini, A., Balduzzi, F., Peiró, J., Graham, J. M. R., Ferrara, G., and Ferrari, L., “On the influence of virtual camber effect on airfoil polars for use in simulations of Darrieus wind turbines,” *Energy Conversion and Management*, Vol. 106, 2015, pp. 373–384.
- [42] Bianchini, A., Balduzzi, F., Rainbird, J. M., Peiro, J., Graham, J. M. R., Ferrara, G., and Ferrari, L., “An Experimental and Numerical Assessment of Airfoil Polars for Use in Darrieus Wind Turbines: Part 1—Flow Curvature Effects,” *Turbo Expo: Power for Land, Sea, and Air*, Vol. 56802, American Society of Mechanical Engineers, 2015, p. V009T46A006.
- [43] Drela, M., “XFOIL: An analysis and design system for low Reynolds number airfoils,” *Low Reynolds number aerodynamics*, Springer, 1989, pp. 1–12.
- [44] Montgomerie, B., “Methods for root effects, tip effects and extending the angle of attack range to ± 180 , with application to aerodynamics for blades on wind turbines and propellers,” *FOI, Swedish Defence Research Agency, Stockholm, Sweden, Report No. FOI*, 2004.
- [45] Shubham, S., Wright, N., and Ianakiev, A., “Application of Richardson extrapolation method to aerodynamic and aeroacoustic characteristics of low Reynolds number vertical axis wind turbines,” *28th AIAA/CEAS Aeroacoustics 2022 Conference*, 2022, p. 3022.
- [46] Qian Cheng, H. S. J. K. C. K. B. Y., Xiaolan Liu, “Aerodynamic Analysis of a Helical Vertical Axis Wind Turbine,” 2017.
- [47] S.M.H. Karimian, A. A., “Performance investigation of a new Darrieus Vertical Axis Wind Turbine,” 2019.
- [48] Unnikrishnan Divakaran, A. M. R. K. V., Ajith Ramesh, “Effect of Helix Angle on the Performance of Helical Vertical Axis Wind Turbine,” 2021.
- [49] Sheldahl, R. E., and Klimas, P. C., “Aerodynamic characteristics of seven symmetrical airfoil sections through 180-degree angle of attack for use in aerodynamic analysis of vertical axis wind turbines,” Tech. rep., Sandia National Labs., Albuquerque, NM (USA), 1981.
- [50] Avallone, F., Ragni, D., and Casalino, D., “On the effect of the tip-clearance ratio on the aeroacoustics of a diffuser-augmented wind turbine,” *Renewable Energy*, Vol. 152, 2020, pp. 1317–1327.
- [51] Lignarolo, L., Ragni, D., Scarano, F., Ferreira, C. S., and Van Bussel, G., “Tip-vortex instability and turbulent mixing in wind-turbine wakes,” *Journal of Fluid Mechanics*, Vol. 781, 2015, pp. 467–493.

2024-01-04

Effect of blade shape on aerodynamic and aeroacoustic characteristics of vertical axis wind turbines using mid-fidelity and high-fidelity methods

Thambidurai Arasi, Tarun Ramprakash

AIAA

Thambidurai Arasi TR, Shubham S, Ianakiev A. (2024) Effect of blade shape on aerodynamic and aeroacoustic characteristics of vertical axis wind turbines using mid-fidelity and high-fidelity methods. In: AIAA SCITECH 2024 Forum, 8-12 January 2024, Orlando, USA, Paper number AIAA 2024-1488

<https://doi.org/10.2514/6.2024-1488>

Downloaded from Cranfield Library Services E-Repository